DRAFT VERSION JANUARY 23, 2020
Typeset using LaTeX **twocolumn** style in AASTeX62

WASP-4 is accelerating towards the Earth: A Cautionary Tale in the Search for Tidal Orbital Decay

L. G. BOUMA,[1] J. N. WINN,[1] R. A. MATSON,[2] H. ISAACSON,[3] A. W. HOWARD,[4] S. B. HOWELL,[2] AND H. KNUTSON[5]

[1] *Department of Astrophysical Sciences, Princeton University, 4 Ivy Lane, Princeton, NJ 08540, USA*
[2] *NASA Ames Research Center, Moffett Field, CA 94035, USA*
[3] *Astronomy Department, University of California, Berkeley, CA 94720, USA*
[4] *Cahill Center for Astrophysics, California Institute of Technology, Pasadena, CA 91125, USA*
[5] *Division of Geological and Planetary Sciences, California Institute of Technology, Pasadena, CA 91125, USA*

(Received January 23, 2020; Revised —; Accepted —)

Submitted to AAS journals.

ABSTRACT

We recently noted that combining measurements from the Transiting Exoplanet Survey Satellite (TESS) with ground-based transit observations, the orbital period of WASP-4b seemed to be decreasing. Possible explanations included tidal orbital decay, orbital precession, and light-travel time effects. In this work we present new observations of the radial velocity of WASP-4, acquired with Keck-HIRES. They show that the system is accelerating towards our line of sight, at $\dot{\gamma} = X.XX \pm Y.YY$ m s^{-1} yr^{-1}. This implies a period decrease of X.XX milliseconds per year, compared to the observed value of Y.YY. Combining the radial velocities with new speckle imaging from Gemini-Zorro, we show that the acceleration is best explained by a 10-200 $M_{\rm Jup}$ companion between 10 and 100 AU. We encourage further long-term monitoring of hot Jupiter radial velocities; these observations are critical in the ongoing hunt for tidal orbital decay.

Keywords: Exoplanet tides (497), Exoplanet dynamics (490), Radial velocity (1332), Transit timing variation method (1710)

1. INTRODUCTION

Since the first discovery of transiting hot Jupiters, the hunt for tidal orbital decay has received much attention (CITE LIKE 20 PAPERS). These efforts are gradually beginning to yield fruit: by combining transit and occultation timing and radial velocity measurements, CITE Yee et al. have shown that the data for the hot Jupiter WASP-12b are most compatible with orbital decay.

The present study highlights a point that, while obvious, has perhaps not yet received due attention. The point is that the hunt for orbital decay of hot Jupiters will be crippled without long-term radial velocity monitoring programs. The reason is simple: when the timescale of orbital period change far exceeds the observing baseline, the first deviation from constant periodicity is always quadratic in the transit number:

$$t_{\rm tra} = t_0 + PE + \frac{1}{2}\frac{dP}{dE}E^2, \quad (1)$$

where

$$\frac{dP}{dE} = P\frac{dP}{dt}, \quad (2)$$

E is the transit number, P is the orbital period, t_0 is the reference epoch, and $t_{\rm tra}$ is the transt mid-time.

There are ample reasons to expect orbital decay to be common (CITE). However there are reasons to expect the Rómer delay to perhaps be even *more* common (CITE Knutson 14, Bryan 16). Both manifest to first order identically in transit times (up to the sign of the line-of-sight acceleration) – as a non-zero period derivative.

Specifically, Knutson et al. (2014) showed that X% of hot Jupiters show some form of radial acceleration in radial velocity time-series with baselines of YY years. Assuming a separation distribution of (WHATEVER), this implies that ZZ% of hot Jupiters will *always* show a changing orbital period, over timescale of say 10 years.

This is specific to hot Jupiters. The abundance of giant planets exterior to Super-Earth sized systems is also high (CITE Bryan 2019).

The main focus of this study is the hot Jupiter WASP-4b, which has an orbital period that from transits appears to be decreasing by about 10 milliseconds per year. After discovering the timing variations in the TESS data (Bouma et al.

Corresponding author: L. G. Bouma
luke@astro.princeton.edu

2019, hereafter B19), we obtained N additional radial velocity measurements using Keck-HIRES, extending the RV baseline by Y years. Previously, the radial velocities were sparse and were consistent with not showing any linear trend. Our new measurements reveal a line of sight acceleration of $\dot{\gamma} = -XX\,\mathrm{m\,s^{-1}\,yr^{-1}}$. This translates to an expected period decrease simply from the light travel time effect of ZZ milliseconds per year — about what is observed.

Thereafter, Southworth et al. (2019) reported 22 new transit times for the system, and confirmed that the updated series of transit times was consistent with a quadratic ephemeris. Their interpretation of the timing variations did not differ in any major respects from our own, though with additional data they found a lower best-fit decay rate of $\dot{P} = -XX.X \pm X.X$ milliseconds per year.

A separate study by **?** reported additional light curves. **?** analyzed their newly obtained photometry, along with archival light curves that we omitted from our analysis due to systematic uncertainties in the absolute time system. **?** found that when they used all the available TTV data, the need for a quadratic ephemeris was present "at the high $\sim 5-7$ sigma level". However, they pointed out that if they used lower-precision subsets of the available timing data, the necessity for the quadratic term decreased. **?** also pointed out that the precise transit times reported by Huitson et al. (2017) were quite important in the time-series. Overall, **?** did not find the claim of a period decrease convincing.

§ 2 presents the new observations... § 3 describes our analysis... § 4 discusses... § **??** gives conclusions...

2. OBSERVATIONS

2.1. *Transits*

Table N lists the transit times we used in our analysis. We include data from the peer-reviewed literature for which (a) the analysis was based on observations of a single transit, (b) the midpoint was fitted as a free parameter, and (c) the time system specified both the absolute reference (TDB or UTC) and also whether any barycentric or heliocentric corrections had been performed.

The majority of times are identical to those we collected in B19. Twenty-two new times reported by Southworth et al. (2019) are included. These transits were observed from the 3.58m NTT and Danish 1.54m telescopes at La Silla, and the SAAO 1.0m telescope.

A number of additional times were also recently reported by Baluev et al. (2019), based on a homogeneous analysis of archival ground-based observations. We included their "high quality" transit times with provenance from the TRAPPIST and El Sauce telescopes, for which we verified with the original observers that appropriate time-system corrections had been performed (M. Gillon, P. Evans, priv. comm.).

The four available occultation data points tabulated by B19 are sparse and have neglegible statistical value due to their large uncertainties, and we forgo their use in this analysis.

2.2. *Radial velocities*

After identifying the period decrease in B19, we acquired four additional radial velocity measurements with the Keck High Resolution Echelle Spectrometer (HIRES, Vogt et al. 1994). Our observations were acquired under the purview of the California Planet Survey (Howard et al. 2010). The spectra were reduced using **software X**. Previously, the HIRES data-points spanned 2010 to 2013 (Knutson et al. 2014). Our new measurements triple the HIRES observing baseline to nine years.

The complete set of radial velocity observations is given in **Table M**. Along with the 2010-2019 HIRES observations, there are also earlier measurements from CORALIE and HARPS. Following B19, we included the CORALIE measurements from Wilson et al. (2008) and Triaud et al. (2010), using the homogeneous radial velocities calculated by the latter authors. We included the HARPS values reported by Pont et al. (2011) and Husnoo et al. (2012). We omitted the HARPS data points taken over three nights by Triaud et al. (2010) for Rossiter-McLaughlin observations because they have a systematic offset from the remaining datasets.

2.3. *Speckle imaging*

A cursory analysis of the new HIRES observations led to our detection of a linear trend in the residuals after fitting out the orbit of WASP-4b. This prompted us to acquire speckle imaging using Zorro at Gemini-South (see Scott et al. 2018, , and the instrument web-pages[1]). Zorro (and its counterpart, 'Alopeke, on Gemini-North) are dual-channel speckle interferometers that can be used to observe in narrow-band filters centered at 562 nm and 832 nm.

We observed WASP-4 twice, on the night of September 11-12 (8 sets of 1000 frames each) and also on the night of September 28-29 (7 sets of 1000 frames each). The second night had better seeing and produced a slightly better result, which we opt to use for our analysis.

We reduced the speckle images to contrast curves by ...

3. ANALYSIS

3.1. *Transits*

We considered two possible models for the observed transit times. The first model assumes a constant orbital period on a circular orbit:

$$t_{\mathrm{tra}}(E) = t_0 + PE, \tag{3}$$

$$\tag{4}$$

where E is the epoch number and t_0 is a reference epoch. The second model assumes the period changes at a steady rate:

$$t_{\mathrm{tra}}(E) = t_0 + PE + \frac{1}{2}\frac{\mathrm{d}P}{\mathrm{d}E}E^2. \tag{5}$$

The free parameters are the reference epoch t_0, the period at the reference epoch, and the period derivative, $\mathrm{d}P/\mathrm{d}t =$

[1] www.gemini.edu/sciops/instruments/alopeke-zorro/

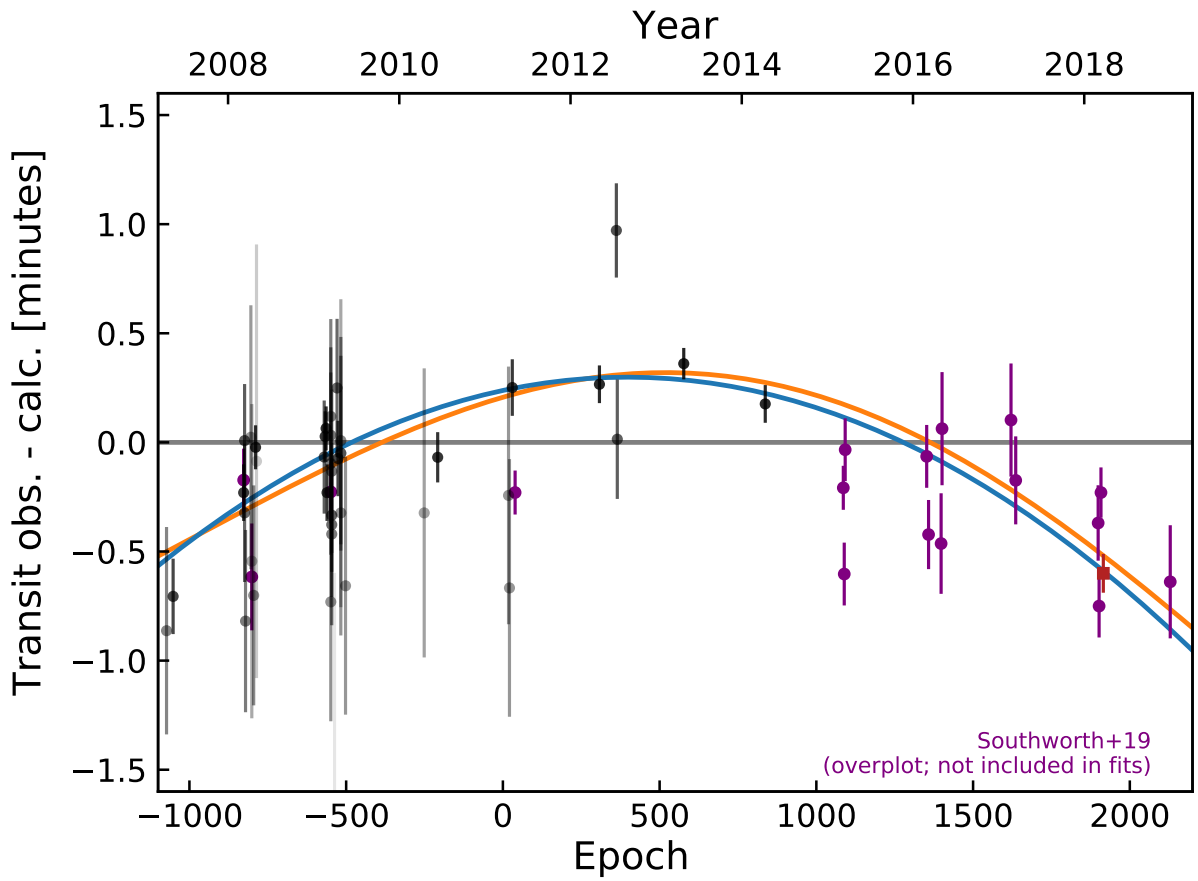

Figure 1. Timing residuals and best-fit models for WASP-4b. The vertical axis shows the observed times minus the calculated times assuming a constant orbital period . Darker points correspond to more precise data. The quadratic ephemeris and its 1σ uncertainties are shown in blue. The binned TESS point (red square) is the weighted average of 18 TESS transits and is for display purposes only. The models were fitted to all of the individual transit times.

$(1/P)\mathrm{d}P/\mathrm{d}E$. We defined the epoch numbers such that $E = 0$ is near the weighted average of the observed times. This helps to reduce the covariance between t_0 and P. A third possible model that we did not consider for reasons that will become apparent is a precessing, eccentric orbit (*e.g.*, Giménez & Bastero 1995; Patra et al. 2017).

We fitted each of the two models by assuming a Gaussian likelihood and sampling over the posterior probability distributions. We sampled the posterior using the algorithm proposed by Goodman & Weare (2010) and implemented by Foreman-Mackey et al. (2013) in `emcee`. The prior for the quadratic model allowed the period derivative to have any sign.

Figure 1 shows the observed transit times, minus the best-fit constant period model. The best-fitting constant-period model has $\chi^2 = XXX$ and YY degrees of freedom. The best-fitting quadratic model has $\chi^2 = YYY$ and ZZ degrees of freedom. The difference in the BIC (Kass & Raftery 1995) between the linear and quadratic and models is $\Delta\mathrm{BIC} = ZZ.Z$, strongly favoring the quadratic case.

The best-fit period derivative in the quadratic model is

$$\dot{P} = -(X.XX \pm 0.XX) \times 10^{-10} = -YY.Y \pm Z.Z \ \mathrm{ms\,yr^{-1}}. \quad (6)$$

This agrees with the value reported by Southworth et al. (2019) after their including an additional 22 archival transit measurements ($\dot{P} = -9.2 \pm 1.1$ ms yr^{-1}). It is smaller than the rate of period decrease found by B19 (-12.6 ± 1.2 ms yr^{-1})., presumably because of missing coverage filled in by Southworth et al.'s observations. The other best-fit transit timing model parameters are reported in **Table X**.

3.2. *Radial Velocities: WASP-4's acceleration towards the Earth*

We began by fitting a single Keplerian orbit, plus instrument offsets, jitters, and a long-term trend (Fulton et al. 2018, `radvel`). We set Gaussian priors on the period and time of inferior conjunction using the values from Table 4 of B19, and fixed the eccentricity to zero, per the results of Beerer et al. (2011), Knutson et al. (2014) and Bonomo et al. (2017). The free parameters were the velocity semi-amplitude, the instrument zero-points, the instrument jitters (an additive white noise term for each instrument), linear ($\dot{v}_\mathrm{r}$), and optionally second-order ($\ddot{v}_\mathrm{r}$) acceleration terms.

We found that the best-fitting model with both linear and quadratic radial velocity terms was marginally preferred (by $\Delta\mathrm{BIC} = 5.8$) over the best-fitting model with only a linear

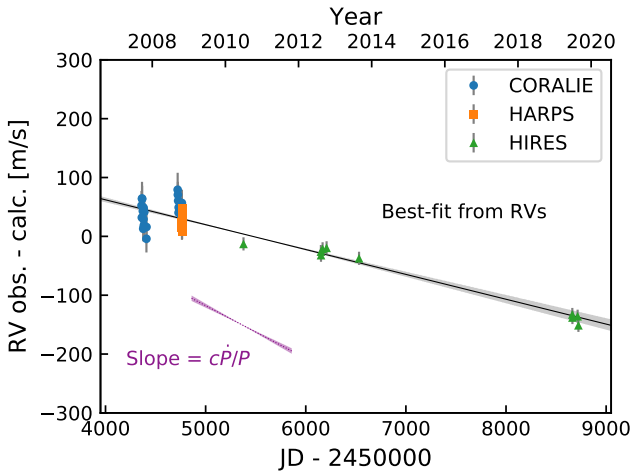

Figure 2. Radial velocity observations of WASP-4. The best-fit Keplerian orbit of WASP-4b has been subtracted. The linear trend inferred from the RV data is shown with a black line, with 1σ errors in gray. The trend that would be needed to produce the period decrease seen in transits ($\dot{P} = -YY.Y \pm Z.Z$ ms yr^{-1}) is indicated with the purple dotted line. The four new RV measurements presented in this work increased the significance of the slope from $\approx 2\sigma$ to 15σ.

term. Regardless, for consistency with Knutson et al. (2014), who fixed the quadratic component of the long-term trend to zero, in Figure 2 we show best-fitting models for the linear-trend case.

WASP-4 was found to be accelerating towards our line of sight at high confidence,

$$\dot{v}_r = -0.0422^{+0.0028}_{-0.0027}\,\mathrm{m\,s^{-1}\,day^{-1}}. \quad (7)$$

For comparison, before our recent observing run, $\dot{v}_r$ was thought to be about five times smaller, and was only marginally significant (Knutson et al. 2014; Bouma et al. 2019).

The system's acceleration towards our line of sight causes a decrease in the apparent orbital period (the Rømer delay). The period derivative expected from radial velocities is

$$\dot{P}_{RV} = \frac{\dot{v}_r P}{c} \quad (8)$$

$$\dot{P}_{RV} = -5.94 \pm 0.39\ \mathrm{ms\,yr^{-1}}. \quad (9)$$

In other words, the majority of the period decrease observed in transits ($\dot{P} = -X.X \pm 1.1$ ms yr^{-1}) seems to be explained by the acceleration of the host star. All the available TTV data show a period decrease of $\approx 8-12$ milliseconds per year (**?**Southworth et al. 2019; **?**).

An important consideration is whether the measured RV trend is at all correlated with stellar activity. We investigate this by analyzing WASP-4's emission in the Ca II H & K lines, as quantified with the chromospheric S-index (Wright et al. 2004). We only examined the HIRES velocities for this step, since they are the main source of signal for our analysis. First, we subtracted the orbital solution from the Keck-HIRES velocities. Then, following Bryan et al. (2016, 2019), we calculated the Spearman rank correlation coefficient between the S-index and the orbit-subtracted velocities. We found a correlation coefficient of 0.16. Though suggestive, it is not statistically significant (the corresponding p-value is 0.65). Furthermore, inspection of the S-index time-series showed no secular or sinusoidal trends, as would be expected if we were observing a long-term magnetic activity cycle. The S-index values are included in **Table X**. We conclude that it would be highly unlikely for the linear trend to be caused by stellar activity.

3.3. *Constraints on companion masses and semi-major axes*

Given a linear radial velocity trend, we can place lower-limits on the mass and semi-major axis of additional bodies in the system. The constraints on the two parameters are degenerate: $\dot{\gamma} \propto M_p a^{-2}$. Nonetheless, the Zorro images and contrast curves can limit the available parameter space by setting an upper limit on the semimajor axis, and a maximum brightness (and thereby mass) of any putative companions.

The general procedure we use to derive constraints on possible companion masses and semi-major axes has been developed by Wright et al. (2007), Crepp et al. (2012), Montet et al. (2014), Knutson et al. (2014), Bryan et al. (2016, 2019), and others.

Speckle imaging constraints—First, we would like to convert the contrast ratios obtained through the Zorro imaging (Figure 3) to limits on the masses of putative companions and their separations from the host star.

To do this, we followed Montet et al. (2014), and opted to employ the Baraffe et al. (2003) models for substellar mass objects and the MIST isochrones for stellar mass objects (Paxton et al. 2011, 2013, 2015; Dotter 2016; Choi et al. 2016). We assumed that the system age was 5 Gyr, so that companions would have fully contracted.

Due to the custom filters of the Zorro imager, and corresponding lack of synthetic photometry, we further assumed that all sources had blackbody spectra. While this is clearly false, we do not readily have access to the planetary and stellar atmosphere models needed for the consistent calculation with the `COND03` and `MESA` models. We therefore adopted the effective temperatures and bolometric luminosities from the Baraffe et al. (2003) and MIST isochrones. Using these theoretical quantities and the empircal Zorro bandpass functions, we calculated absolute magnitudes in the 562 and 832 nm Zorro bandpasses for stellar and planetary mass companions. Applying the same calculation to WASP-4 itself using the effective temperature and bolometric luminosity from B19, we derived the transformation from contrast ratio to companion mass. The resulting limits are shown as the cross-hatched region in Figure 4.

Radial velocity constraints—To derive constraints on possible companion masses and separations from the radial velocities, we followed the procedure of Bryan et al. (2019). We began by defining a 50×50 grid in true planetary mass and semimajor axis, evenly spaced from 1 to $300\,M_{Jup}$ and 3 to 500 AU.

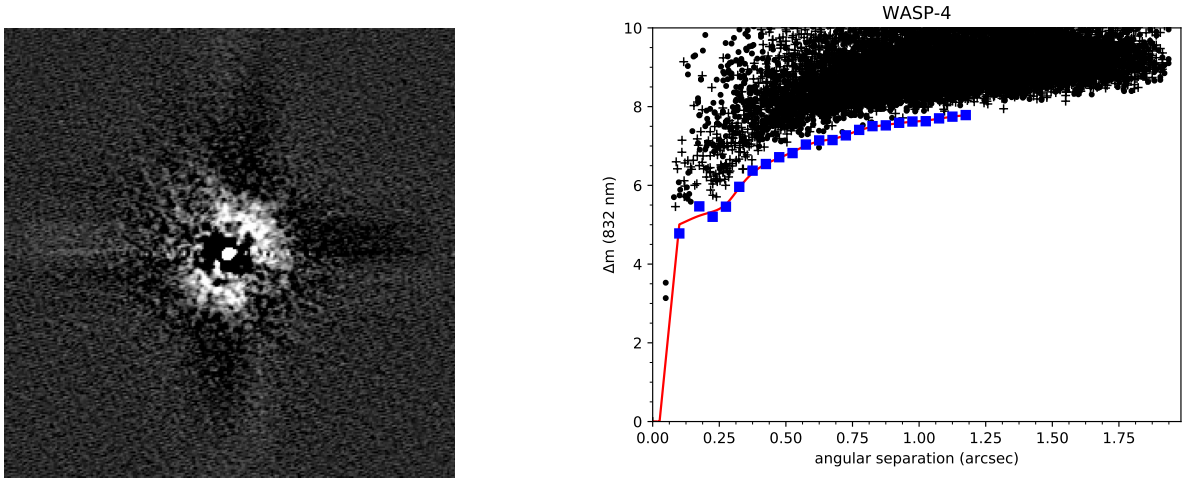

Figure 3. *Left:* Speckle image reconstructed from 1000 40 millisecond frames in an 832 nm bandpass, and acquired on September 28, 2019. The image scale is $2.46'' \times 2.46''$. *Right:* Contrast curve derived from point-source injection-recovery experiments.

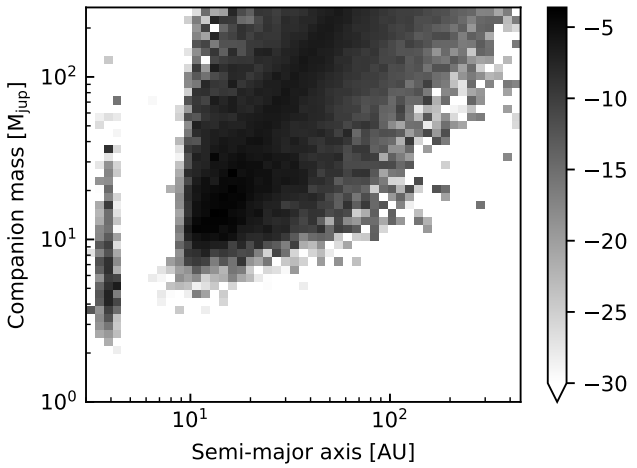

Figure 4. Masses and semi-major axes of companions that meet requirements of both the radial velocity and the speckle imaging. The likelihood inferred from radial velocities is shown in grayscale, and the region excluded from the imaging is shown with a cross-hatch pattern.

We then considered the possibility that an additional companion in any particular cell could explain the observed linear trend. In each cell, we simulated 500 hypothetical companions.

We assigned each companion a mass and semimajor axis from log-uniform distributions within the grid cell. We drew the inclination from a uniform distribution in $\cos i$. The eccentricity was drawn from Kipping (2013)'s long-period exoplanet Beta distribution ($a = 1.12$, $b = 3.09$). For each simulated companion, we then drew a sample from the converged chains of our initial model of WASP-4b, plus its linear trend. We subtracted the planet's orbital solution, leaving the linear trend. Given $(a_c, M_c, e_c$ for each simulated outer companion, and the fixed instrument offsets and jitters from the MCMC chains, we then performed a maximum likelihood fit for the time and argument of periastron of the outer simulated companion. We converted the resulting $50 \times 50 \times 500$ cube of best-fit log-likelihood values to probabilities, and averaged over the samples in each grid cell to derive a probability distribution in mass and semi-major axis.

The result is shown as grayscale background in Figure 4.

4. DISCUSSION

4.1. *Implications for WASP-4*

Previous possibilities suggested to explain the period decrease of WASP-4b included tidal orbital decay, orbital precession, and light-travel time effects (Bouma et al. 2019). Our new radial velocity measurements have now shown the least exotic option—light-travel time effects—is also the most likely explanation. Transits show the obital period to decrease by $YY.Y \pm Z.Z$ ms yr^{-1}; the line-of-sight acceleration observed in radial velocities implies an expected period decrease of $YY.Y \pm Z.Z$ ms yr^{-1}. Though the quantitative agreement is not perfect, Occam's razor would suggest that the line of sight acceleration is probably a sufficient explanation for the apparent decrease of WASP-4b's orbital period.

The corresponding requirements for the companion causing the acceleration are that it is likely either a brown-dwarf or low mass star, and that it is between 10-100 AU from the host star (Figure 4). Given such a mass, this companion could at one time have influenced the orbital evolution of the inner giant. Further radial velocity monitoring should eventually reveal the orbital parameters and minimum mass of the companion.

4.2. *How many other hot Jupiters will show the Rómer delay?*

We identified WASP-4b's decreasing orbital period as part of a search for tidal orbital decay. However, over half of hot Jupiters have companions outside of 1 AU with super-Jovian

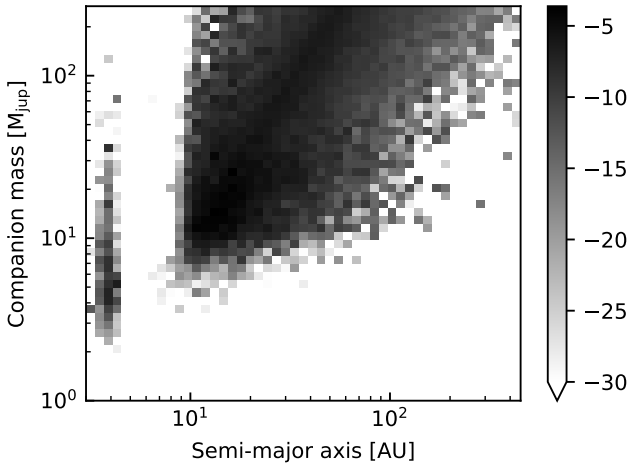

Figure 5. ...

masses (Knutson et al. 2014). Line-of-sight accelerations are therefore relatively common in hot Jupiter systems.

To evaluate the importance of these effects in future transit timing searches, we collected the linear trends reported by Knutson et al. (2014), and computed the expected orbital period changes $\dot{P}_{\rm RV} = \dot{v}_{\rm r} P/c$ for all the systems. The results are given in **Table X**, and visualized for hot Jupiters with significant linear trends in Figure 5.

5. CONCLUSIONS

This paper includes data collected by the TESS mission, which are publicly available from the Mikulski Archive for Space Telescopes (MAST). Funding for the TESS mission is provided by NASA's Science Mission directorate. This work made use of NASA's Astrophysics Data System Bibliographic Services. Based on observations obtained at the Gemini Observatory, which is operated by the Association of Universities for Research in Astronomy, Inc., under a cooperative agreement with the NSF on behalf of the Gemini partnership: the National Science Foundation (United States), National Research Council (Canada), CONICYT (Chile), Ministerio de Ciencia, Tecnología e Innovación Productiva (Argentina), Ministério da Ciência, Tecnologia e Inovação (Brazil), and Korea Astronomy and Space Science Institute (Republic of Korea). Observations in the paper made use of the High-Resolution Imaging instrument Zorro at Gemini-South. Zorro was funded by the NASA Exoplanet Exploration Program and built at the NASA Ames Research Center by Steve B. Howell, Nic Scott, Elliott P. Horch, and Emmett Quigley. This research has made use of the VizieR catalogue access tool, CDS, Strasbourg, France. The original description of the VizieR service was published in A&AS 143, 23. This work has made use of data from the European Space Agency (ESA) mission *Gaia* (https://www.cosmos.esa.int/gaia), processed by the *Gaia* Data Processing and Analysis Consortium (DPAC, https://www.cosmos.esa.int/web/gaia/dpac/consortium). Funding for the DPAC has been provided by national institutions, in particular the institutions participating in the *Gaia* Multilateral Agreement.

Software: `astrobase` (Bhatti et al. 2018), `astroplan` (Morris et al. 2018), `astropy` (Collaboration et al. 2018), `astroquery` (Ginsburg et al. 2018), `corner` (Foreman-Mackey 2016), `emcee` (Foreman-Mackey et al. 2013), `IPython` (Pérez & Granger 2007), `matplotlib` (Hunter 2007), `MESA` (Paxton et al. 2011, 2013, 2015) `numpy` (Walt et al. 2011), `pandas` (McKinney 2010), `radvel` (Fulton et al. 2018), `scipy` (Jones et al. 2001).

Table 4. Best-fit transit timing model parameters.

Parameter	Median Value (Unc.)[a]
Constant period	
t_0 [BJD$_{\rm TBD}$]	2455804.515752(+19)(-19)
P [days]	1.338231466(+23)(-22)
Constant period derivative	
t_0 [BJD$_{\rm TBD}$]	2455804.515918(+24)(-24)
P [days]	1.338231679(+31)(-31)
dP/dt	$-4.00(+37)(-38) \times 10^{-10}$

[a] **FIXME table needs numbers** The numbers in parenthesis give the 68% confidence interval for the final two digits, where appropriate.

REFERENCES

Baluev, R. V., Sokov, E. N., Jones, H. R. A., et al. 2019, arXiv:1908.04505 [astro-ph], arXiv: 1908.04505

Baraffe, I., Chabrier, G., Barman, T. S., Allard, F., & Hauschildt, P. H. 2003, Astronomy and Astrophysics, 402, 701

Beerer, I. M., Knutson, H. A., Burrows, A., et al. 2011, The Astrophysical Journal, 727, 23

Bhatti, W., Bouma, L. G., & Wallace, J. 2018, `astrobase`

Bonomo, A. S., Desidera, S., Benatti, S., et al. 2017, Astronomy and Astrophysics, 602, A107

Bouma, L. G., Winn, J. N., Baxter, C., et al. 2019, The Astronomical Journal, 157, 217

Bryan, M. L., Knutson, H. A., Lee, E. J., et al. 2019, The Astronomical Journal, 157, 52

Bryan, M. L., Knutson, H. A., Howard, A. W., et al. 2016, The Astrophysical Journal, 821, 89

Choi, J., Dotter, A., Conroy, C., et al. 2016, The Astrophysical Journal, 823, 102, arXiv: 1604.08592

Collaboration, T. A., Price-Whelan, A. M., Sipöcz, B. M., et al. 2018, arXiv:1801.02634 [astro-ph], arXiv: 1801.02634

Crepp, J. R., Johnson, J. A., Howard, A. W., et al. 2012, The Astrophysical Journal, 761, 39

Dotter, A. 2016, The Astrophysical Journal Supplement Series, 222, 8

Foreman-Mackey, D. 2016, The Journal of Open Source Software, 24

Foreman-Mackey, D., Hogg, D. W., Lang, D., & Goodman, J. 2013, Publications of the Astronomical Society of the Pacific, 125, 306

Fulton, B. J., Petigura, E. A., Blunt, S., & Sinukoff, E. 2018, arXiv:1801.01947 [astro-ph], arXiv: 1801.01947

Giménez, A., & Bastero, M. 1995, Astrophysics and Space Science, 226, 99

Ginsburg, A., Sipocz, B., Madhura Parikh, et al. 2018, Astropy/Astroquery: V0.3.7 Release

Goodman, J., & Weare, J. 2010, Communications in Applied Mathematics and Computational Science, 5, 65

Howard, A. W., Johnson, J. A., Marcy, G. W., et al. 2010, The Astrophysical Journal, 721, 1467

Huitson, C. M., Désert, J.-M., Bean, J. L., et al. 2017, The Astronomical Journal, 154, 95

Hunter, J. D. 2007, Computing in Science & Engineering, 9, 90

Husnoo, N., Pont, F., Mazeh, T., et al. 2012, Monthly Notices of the Royal Astronomical Society, 422, 3151

Jones, E., Oliphant, T., Peterson, P., et al. 2001, Open source scientific tools for Python

Kass, R. E., & Raftery, A. E. 1995, Journal of the American Statistical Association, 90, 773

Kipping, D. M. 2013, Monthly Notices of the Royal Astronomical Society: Letters, 434, L51

Knutson, H. A., Fulton, B. J., Montet, B. T., et al. 2014, The Astrophysical Journal, 785, 126

McKinney, W. 2010, in Proceedings of the 9th Python in Science Conference, ed. S. van der Walt & J. Millman, 51

Montet, B. T., Crepp, J. R., Johnson, J. A., Howard, A. W., & Marcy, G. W. 2014, The Astrophysical Journal, 781, 28

Morris, B. M., Tollerud, E., Sipőcz, B., et al. 2018, AJ, 155, 128

Patra, K. C., Winn, J. N., Holman, M. J., et al. 2017, The Astronomical Journal, 154, 4

Paxton, B., Bildsten, L., Dotter, A., et al. 2011, The Astrophysical Journal Supplement Series, 192, 3

Paxton, B., Cantiello, M., Arras, P., et al. 2013, The Astrophysical Journal Supplement Series, 208, 4

Paxton, B., Marchant, P., Schwab, J., et al. 2015, The Astrophysical Journal Supplement Series, 220, 15

Pérez, F., & Granger, B. E. 2007, Computing in Science and Engineering, 9, 21

Pont, F., Husnoo, N., Mazeh, T., & Fabrycky, D. 2011, Monthly Notices of the Royal Astronomical Society, 414, 1278

Scott, N. J., Howell, S. B., Horch, E. P., & Everett, M. E. 2018, Publications of the Astronomical Society of the Pacific, 130, 054502

Southworth, J., Dominik, M., Jorgensen, U. G., et al. 2019, arXiv:1907.08269 [astro-ph], arXiv: 1907.08269

Triaud, A. H. M. J., Collier Cameron, A., Queloz, D., et al. 2010, Astronomy and Astrophysics, 524, A25

Vogt, S. S., Allen, S. L., Bigelow, B. C., et al. 1994, in , 362

Walt, S. v. d., Colbert, S. C., & Varoquaux, G. 2011, Computing in Science & Engineering, 13, 22

Wilson, D. M., Gillon, M., Hellier, C., et al. 2008, The Astrophysical Journal Letters, 675, L113

Wright, J. T., Marcy, G. W., Butler, R. P., & Vogt, S. S. 2004, The Astrophysical Journal Supplement Series, 152, 261

Wright, J. T., Marcy, G. W., Fischer, D. A., et al. 2007, The Astrophysical Journal, 657, 533